

Convective Dynamos and the Minimum X-ray Flux in Main Sequence Stars

D. J. Bercik¹, G. H. Fisher¹, Christopher M. Johns-Krull² and W. P. Abbett¹

¹ *Space Sciences Laboratory, University of California, Berkeley, CA 94720-7450*

² *Department of Physics and Astronomy, Rice University, 6100 Main St., MS-108, Houston, TX 77005*

ABSTRACT

The objective of this paper is to investigate whether a convective dynamo can account quantitatively for the observed lower limit of X-ray surface flux in solar-type main sequence stars. Our approach is to use 3D numerical simulations of a turbulent dynamo driven by convection to characterize the dynamic behavior, magnetic field strengths, and filling factors in a non-rotating stratified medium, and to predict these magnetic properties at the surface of cool stars. We use simple applications of stellar structure theory for the convective envelopes of main-sequence stars to scale our simulations to the outer layers of stars in the F0–M0 spectral range, which allows us to estimate the unsigned magnetic flux on the surface of non-rotating reference stars. With these estimates we use the recent results of Pevtsov et al. (2003) to predict the level of X-ray emission from such a turbulent dynamo, and find that our results compare well with observed lower limits of surface X-ray flux. If we scale our predicted X-ray fluxes to Mg II fluxes we also find good agreement with the observed lower limit of chromospheric emission in K dwarfs. This suggests that dynamo action from a convecting, non-rotating plasma is a viable alternative to acoustic heating models as an explanation for the basal emission level seen in chromospheric, transition region, and coronal diagnostics from late-type stars.

Subject headings: stars: magnetic fields — activity

1. Introduction

Understanding the origin of magnetic activity in stars has been an important research area in astronomy and astrophysics for many years. Imaged solar observations show a clear

link between magnetic fields and the formation of heated plasma in the chromosphere, transition region and corona, especially in active regions (see Fisher et al. 1998). Active regions are believed to form from loops of magnetic flux that emerge from the base of the solar convection zone (see e.g., reviews by Fisher et al. 2000; Fan 2004 ¹). The large-scale magnetic field on the Sun is believed to originate via a global-scale dynamo, powered mainly by the velocity shear (differential rotation) between the convection zone and the radiative interior. It is often assumed that the amount of differential rotation increases as the rotation rate itself increases. For example, theoretical studies of differential rotation mechanisms such as the “A effect” (Rüdiger 1989) find that the amount of differential rotation generated by Reynolds stresses is proportional to the rotation rate.

Skumanich (1972) was among the first to propose an observational connection between rotation rate and the level of activity in stars through dynamo action. Noyes et al. (1984) went on to show a clear correlation between the Ca II H+K surface flux and rotation rate, arguing that the correlation is made better with the inclusion of a convective turnover time via the Rossby number. Vilhu (1984) finds a similar result for chromospheric, transition region, and coronal emission diagnostics. Basri (1987) shows that the activity of dwarf and RS CVn stars both correlate well with rotation rate, but with a slight offset between the two classes of stars, while the two classes appear to follow the same relationship when the rotation period is divided by the convective turnover time (see also Johns-Krull, Valenti, & Linsky 2000). These studies provide strong observational support for the existence of the so-called α - Ω dynamo (e.g., Durney & Latour 1978), which relies on the interaction of convection and rotation — specifically, differential rotation (the “ Ω ” effect) and field regeneration by cyclonic motions (the “ α ” effect) — to generate a magnetic field in a fashion similar to that believed responsible for the large-scale solar dynamo.

For cool stars, a straightforward application of the relationship between stellar rotation and magnetic activity described above leads one to conclude that those stars that rotate slowly or do not rotate (hereafter collectively termed “non-rotating stars”) should show little or no activity diagnostics. However, this is not the case. There appears to be a lower limit to the emission of activity indicators in the chromosphere, transition region, and corona. Given the expected absence of a global dynamo in non-rotating stars, this heating is usually attributed to a “basal” non-magnetic mechanism such as heating by acoustic waves. Schrijver (1987) first introduced the term “basal flux density” to refer to that portion of the chromospheric and transition region line emission which results from a process other than the solar-like cyclic dynamo activity (termed “excess” emission).

¹<http://www.livingreviews.org/lrsp-2004-1>

Evidence for a basal flux and the contention that it is acoustic in origin has been based on three observational arguments. First, plots of the Ca II H+K chromospheric flux (as observed in the Mt. Wilson HK project, Vaughan, Preston, & Wilson 1978) versus stellar color show a lower boundary up against which the stellar observations appear to cluster (Rutten 1984; Schrijver 1987; Rutten et al. 1991). Such a lower boundary is also apparent in other diagnostics such as Mg II h and k and Si II (Schrijver 1987) as well as in C II, C IV, and Si IV (Rutten et al. 1991). A second line of analysis examines flux-flux diagrams for samples of stars and seeks to make these as tight as possible by subtracting a color dependent basal emission level from one or more of the diagnostics under consideration (Mewe, Schrijver, & Zwaan 1981; Schrijver 1983, 1987; Schrijver, Dobson, & Radick 1989; Rutten et al. 1991). The basal emission level is suggested to be acoustic in origin, while the “excess” above this level is believed to be magnetic in origin. In cases where a basal flux is determined from these flux-flux studies, its value is similar to the lower limit of the flux found in flux-color diagrams. A third argument for the existence of a basal flux comes from studies connecting rotation and activity. Schrijver, Dobson, & Radick (1989) extrapolate the color dependent rotation-activity relationship in Ca II H+K to zero rotation velocity, finding a non-zero activity level which they identify as the basal flux level. This procedure produces a color dependent basal emission similar in strength to that found from flux-color and flux-flux analyses, and this basal emission is again argued to be non-magnetic in origin.

Theoretical estimates of the acoustic heating of chromospheres have been in the literature for some time (see review by Schrijver 1995). We mention here only some of the more recent results which now show good agreement with the observationally inferred basal emission levels. Buchholz, Ulmschneider, & Cuntz (1998) compute time dependent models of basal heating for monochromatic acoustic wave models, solving the hydrodynamic equations together with the radiative transfer and statistical equilibrium equations in order to predict basal emission levels in both the Ca II H+K and Mg II h+k diagnostics. These models produce the observed dependence of the lower bound of emission with stellar color, though the magnitude of the emission depends rather sensitively on whether complete or partial redistribution is assumed for the line transfer. Unfortunately, partial redistribution works best for Mg II while complete redistribution gives a closer match to the Ca II observations. Mullan & Cheng (1994a,b) extend their acoustic wave models to lower mass column densities and find the formation of a relatively cool corona (~ 0.6 MK) when applied to F stars and to M dwarfs ($T = 0.7\text{--}1.0$ MK). While this temperature for M dwarfs is lower than the coronal temperatures found observationally for both dMe and dM stars (Giampapa et al. 1996), Mullan & Cheng (1994a) do find that their acoustically heated models can produce a surface flux in excess of that observed on the least X-ray active dM stars. Given the relative success of wave propagation models at predicting the basal level of chromospheric

(and possibly coronal) emission, Judge & Carpenter (1998) examined high spectral resolution observations of C II lines in basal level stars and in quiet regions on the Sun to look for evidence of upward propagating shock waves as predicted by acoustic heating models. No such evidence was found, prompting Judge & Carpenter (1998) to call into question the non-magnetic origin for basal emission.

The role of basal flux in the observed X-ray emission is more uncertain observationally compared to chromospheric and transition region diagnostics. The early flux-flux studies (Mewe, Schrijver, & Zwaan 1981; Schrijver 1983, 1987; Schrijver, Dobson, & Radick 1989) did not attempt to find a basal level in soft X-ray emission. Rutten et al. (1991) did find a strongly color dependent lower bound on the X-ray emission of stars in his sample, but this was likely due to instrumental detection limits, as the recent volume limited study by Schmitt (1997) clearly shows that the lower bound on X-ray emission in cool stars has a very weak color dependence at best; which, if it exists, is in the opposite sense to that found by Rutten et al. (1991). While their X-ray data probably suffered from detection limitations, it should be noted that Rutten et al. (1991) do not find a basal level to the X-ray emission — they find that all of the X-ray emission is “excess” in nature, and therefore likely magnetic in origin. In a later study, Mullan & Cheng (1994b) argued that the observed X-ray emission from late A and early F dwarfs is basal (and therefore acoustic) in nature, while Mullan & Cheng (1994a) and Mullan & Fleming (1996) have argued that 90% or more of the X-ray emission from dM stars is basal (acoustic) in origin.

In the more recent, volume-limited study of nearby stars, Schmitt (1997) finds that essentially all stars with outer convection zones emit X-rays with characteristics similar to the solar coronal emission. It seems, therefore, that all “cool stars” possess coronae. Do they then also possess magnetic fields? Schmitt (1997) notes that for the nearby cool stars, there is a well defined minimum X-ray surface flux of $\log F_X \sim 3.7$ (in cgs units) which appears largely independent of stellar color. Such a lower bound to the X-ray emission is reminiscent of the idea of “basal” surface flux in chromospheric and transition region emission in cool stars, which is usually assumed to be acoustic in origin, as noted above. Recent work analyzing both solar and stellar data (Pevtsov et al. 2003) indicates a clear and unambiguous relationship between unsigned magnetic flux and coronal X-ray emission that extends over twelve orders of magnitude. In that paper, observations ranging from small patches of the quiet Sun to the most active pre-main sequence stars were analyzed. At the small-scale end of this study, Kitt Peak magnetograms and Yohkoh SXT images were averaged over a 4 heliographic degree square area centered at the equator and central meridian of the Sun, with reported magnetic fluxes and X-ray fluences normalized to a single arc-second square area on the solar disk, corresponding to the approximate size of a single Kitt Peak magnetogram pixel (Pevtsov 2004). This study lends further credence to the idea that at least for X-ray

emission, a “basal” heating mechanism may indeed be magnetic in origin, but unlike the “excess” emission from global fields, the magnetic flux has little or no connection to stellar rotation.

High resolution observations of the Sun indicate a viable magnetic origin for this “basal” magnetic activity emission: The existence of a small-scale magnetic component which appears to exist independent of the large-scale fields that define the solar cycle, and which had been predicted to be generated locally by turbulent convective motions (Meneguzzi & Pouquet 1986; Durney, De Young, & Roxburgh 1993). Detailed studies of the small-scale magnetic field on the Sun from the MDI instrument on SOHO (Title & Schrijver 1998; Hagenaar, Schrijver, & Title 2003) find strong evidence that small-scale mixed-polarity magnetic concentrations observed in the quiet Sun show only a weak solar-cycle dependence. By studying the detailed evolution of this field over time scales of roughly one day, the authors conclude that this flux is formed by the emergence of small-scale bipoles (e.g., ephemeral active regions, Harvey 1993) and dissipated by flux cancellation, where the collision of two opposite polarities appears to result in their mutual disappearance (Simon, Title, & Weiss 2001; Parnell 2002). Title & Schrijver (1998) estimate a flux replenishment time scale of forty hours, while the more recent study of Hagenaar, Schrijver, & Title (2003) estimate a replenishment time scale of sixteen hours. In any case, the quiet Sun magnetic flux — however it is generated — appears to correctly predict the X-ray fluence for the quiet Sun in the study of Pevtsov et al. (2003). More recent observations (Lin & Rimmele 1999; Khomenko et al. 2003; Bueno, Shchukina, & Ramos 2004) using spectropolarimetric instruments in conditions of extremely good seeing have found evidence of a mixed polarity magnetic field on even smaller, sub-granulation spatial scales. Taken together, these measurements imply that turbulent convection may produce a small-scale mixed polarity field over a very wide range of spatial scales in the Sun.

Complementing the observational evidence for small-scale magnetic fields is a broad base of theoretical work. Research in the field of “fast dynamos” (e.g., Vainshtein et al. 1996; Tanner & Hughes 2003) indicates that in the presence of wide classes of chaotic flow fields, magnetic energy can grow very efficiently, even in the absence of rotation. In these studies, the magnetic induction equation is solved kinematically in the presence of a prescribed flow field. If the fluid streamlines are sufficiently chaotic, the growth of magnetic energy can proceed exponentially quickly. Much of the research in this area focuses on highly idealized flow fields (e.g. Vainshtein et al. 1996) and does not account for the role of the Lorentz force in limiting the growth of the magnetic field.

The major theoretical breakthrough in this area was made by Cattaneo (1999), who demonstrated via a 3D MHD simulation in the Boussinesq approximation that a small seed

field embedded in a turbulently convecting, highly conducting plasma can indeed grow exponentially until the magnetic energy reaches a level of 10–20% of the kinetic energy of the convective motions. Subsequent work by Thelen & Cattaneo (2000) has shown how variation of boundary conditions and fluid mechanics parameters affect the development of the dynamo, while Emonet & Cattaneo (2001) have focused on computing observational diagnostics of the small-scale disordered field.

Turbulent convective dynamo models of this type must not be confused with global-scale dynamo models driven by kinetic helicity in small-scale turbulent motions, which require rotation to generate an α effect. An example of such a model is that of Küker & Rüdiger (1999), who used an α^2 model to understand magnetic field generation in rotating, fully-convective naked T-Tauri stars, which are believed to have little or no differential rotation (Johns-Krull 1996). The idea is that helical turbulence driven by Coriolis forces can impart a systematic twist to field lines encountering the convective eddies, leading eventually to a large-scale steady magnetic field. In contrast, the turbulent dynamo that we believe to be responsible for the small-scale disordered field in the quiet Sun is unaffected by rotation, since the convective turnover time in the topmost layers of the solar convection zone is far smaller than the solar rotation period.

The growing evidence for the importance of small-scale magnetic fields in stellar atmospheres and the observational evidence for a limit to the X-ray emission in stellar coronae leads to the question: Is the turbulent convective dynamo a viable mechanism to generate enough X-ray flux to account for the observational limit? To address this question, in § 2 we extend the investigation of field generation by a turbulent dynamo beyond the Boussinesq approximation into the “anelastic” regime (Gough 1969; Lantz & Fan 1999; Fan et al. 1999) — an approximation to the 3D MHD equations that allows for gravitational stratification while still filtering out acoustic waves. Here, we describe the numerical model and present a detailed analysis of our dynamo simulations. In § 3, we describe our method of utilizing the simulation results to predict the level of X-ray emission in main sequence stars, in § 4 we present our results, and finally in § 5 we discuss the implications of our results and summarize our findings.

2. Description of the Model Dynamo

We solve the 3D system of MHD equations in the anelastic limit (see Lantz & Fan 1999; Fan et al. 1999 and references therein for a description of the anelastic formalism and a discussion of the techniques employed to numerically solve the anelastic system). Briefly, the anelastic approximation results from a scaled variable expansion of the fully-

compressible MHD equations. Density fluctuations in the continuity equation are of high order in the expansion and are neglected — this effectively filters out rapidly propagating acoustic waves, and provides a significant computational savings. The density fluctuations are retained, however, in the buoyancy force term of the momentum equation, which allows for stratification within the computational domain. Thus, the anelastic formulation is an intermediary approximation between a fully-compressible treatment (see e.g., Tobias, et al. 2001; Dorch 2004) and a Boussinesq model (see e.g., Cattaneo 1999). This treatment is well-suited for describing the high- β plasma of stellar interiors, but cannot directly model surface plasmas where $\beta \approx 1$ and the acoustic Mach number becomes large.

In particular, we solve a non-dimensional form of the anelastic MHD equations in a horizontally periodic, vertically closed Cartesian domain. Our non-rotating rectangular box spans five pressure scale heights vertically, which corresponds to a density difference of ~ 20 between the upper and lower boundaries. The resolution of the Cartesian domain is $288 \times 288 \times 72$, which gives an aspect ratio for the box of $4 : 4 : 1$. The non-dimensional parameters R_e and P_r (the Reynolds number and Prandtl number, respectively) are defined as $R_e \equiv \rho_{\text{ref}} v_{\text{conv}} H_{\text{ref}} / \mu$ and $P_r \equiv \mu / \kappa$, and are set to 750 and unity respectively (the Reynolds number was chosen to be as large as possible without introducing numerical artifacts). Here, H_{ref} denotes the pressure scale height at the base of the domain, κ refers to the coefficient of thermal conductivity, and μ is the coefficient of dynamic viscosity (assumed constant). The convective velocity is measured in units of v_{conv} , where $v_{\text{conv}} \equiv (\delta_{\text{ref}} g H_{\text{ref}})^{1/2}$, δ_{ref} is the non-dimensional super-adiabaticity, and g is the constant vertical gravitational acceleration.

We begin by dynamically and thermally relaxing a purely hydrodynamic model convection zone. We initiate convection by introducing a small random entropy perturbation within a computational domain with a prescribed background entropy gradient (see Fan, Abbett, & Fisher 2003; Abbett et al. 2004), and allow the simulation to progress past the time when the convective velocity field attains a statistically steady state. We then set the magnetic Reynolds number $R_m \equiv v_{\text{conv}} H_{\text{ref}} / \eta$ of the simulation to 1000, and introduce a small, dynamically unimportant magnetic seed field (after $t = 164 H_{\text{ref}} / v_{\text{conv}}$ of the field-free relaxation run). The seed field self-consistently grows and evolves within the computational domain as the run progresses (see Figures 1 and 2). The vertical boundary conditions on the magnetic field are stress-free and non-penetrating at the bottom, and the field at the upper boundary is assumed potential. We note that unlike the simulations of Abbett et al. (2004), our potential field upper boundary condition does allow for a small amount of horizontally-directed signed magnetic flux to diffuse out of the domain. Also note that our “global” diffusion timescale of $t_D = 1000 H_{\text{ref}} / v_{\text{conv}}$ — the characteristic time over which a magnetic structure diffuses across H_{ref} (as specified by our choice of magnetic Reynolds number) — greatly exceeds the characteristic convective timescale of the simulation.

Figure 1 shows the temporal evolution of the total kinetic (E_k), thermal (E_{th}), and magnetic (E_B) energy fluctuations (each integrated over the entire domain). The quantities are normalized by the sum of the three ($E_T \equiv E_k + E_{th} + E_B$). We find that the energy of the seed field (initially at 10^{-12} of the total kinetic energy) increases exponentially with a growth time of $\sim 16 H_{\text{ref}}/v_{\text{conv}}$ until the magnetic field becomes dynamically important ($t \approx 350 H_{\text{ref}}/v_{\text{conv}}$), after which the increase becomes approximately linear in time. The magnetic energy fully saturates to a time-averaged value of 6.7% of the total kinetic energy after $t \approx 600 H_{\text{ref}}/v_{\text{conv}}$, and ranges from 5.5–8.5% of E_k . Figure 2 shows the energies on a linear scale — as the magnetic energy increases, the kinetic energy decreases, and the thermal energy fluctuations of the plasma increase. Figure 3 is a volume rendering of both the entropy perturbations (bottom frame) and magnetic field strength $|\mathbf{B}|$ well after the field has saturated ($t = 710 H_{\text{ref}}/v_{\text{conv}}$). It is evident that strong magnetic fields are concentrated in the narrow, low-entropy vortical downdrafts characteristic of stratified convection (particularly in the upper half of the box), and that a greater proportion of the total unsigned magnetic flux resides in the lower half of the box. The net signed flux in our dynamo simulations is always zero, and unless otherwise stated, all magnetic fluxes discussed hereafter refer to unsigned magnetic fluxes. We note that even though our simulations exhibit the vertical flow asymmetries typical of stratified convection, and even though we use different values of dimensionless fluid parameters and do not achieve the highest numerical resolutions explored by Cattaneo (1999), we still find similar and significant levels magnetic energy relative to kinetic energy over the simulation domain. Figure 4 shows a “magnetogram” of the vertical component of the field near the top of the simulation box (left panel) and near the base of the box (right panel).

To quantify the distribution of unsigned magnetic flux in the domain (after the dynamo has fully saturated), we define a magnetic filling factor

$$f = \frac{\int_0^{\mathcal{L}_y} \int_0^{\mathcal{L}_x} N dx dy}{\int_0^{\mathcal{L}_y} \int_0^{\mathcal{L}_x} dx dy}, \quad (1)$$

where \mathcal{L}_x and \mathcal{L}_y refer to the horizontal extent of the Cartesian domain, and the quantity N is defined as unity if $|B_z| \geq |B_z|^{\text{cut}}$ and zero otherwise ($|B_z|^{\text{cut}}$ is a chosen threshold value). If we adopt a threshold value of $|B_z|^{\text{cut}}/|B_z|^{\text{max}} = 0.5$, we find that along horizontal slices near the top and bottom of the domain — $z_u = 2.06 H_{\text{ref}}$ and $z_l = 0.45 H_{\text{ref}}$ respectively — the time average of the filling factor $\langle f \rangle$ varies little, and is quite small: $\langle f(z_u) \rangle = 1.47 \times 10^{-4}$ and $\langle f(z_l) \rangle = 6.09 \times 10^{-5}$. This indicates that strong fields are concentrated and highly localized. Here, $|B_z|^{\text{max}}$ refers to the maximum value of $|B_z|$ at z_u sampled every $5 H_{\text{ref}}/v_{\text{conv}}$ in the time interval between $t = 600$ – $850 H_{\text{ref}}/v_{\text{conv}}$. If we choose a cutoff of $|B_z|^{\text{cut}}/|B_z|^{\text{max}} = 0.05$ we find a much larger disparity for the same horizontal planes:

$\langle f(z_u) \rangle = 0.00473$ near the surface, and $\langle f(z_l) \rangle = 0.149$ near the bottom. This suggests that the weaker field is more evenly distributed, particularly in the lower half of the domain. Figure 5 shows the time averaged filling factor as a function of $|B_z|^{\text{cut}}/|B_z|^{\text{max}}$ along both slices. The dashed and dotted lines denote the horizontal planes near the surface and closer to the lower boundary respectively (these planes are the same as those shown in Figure 4). The solid line denotes the time averaged volumetric filling factor (the volumetric analogue to the area filling factor with $|B_z|^{\text{max}}$ defined as the maximum value of $|B|$ in the volume).

A topic of great current interest is the dependence of dynamo behavior on the magnetic Prandtl number P_m , which is the ratio of kinematic viscosity to magnetic diffusivity, (or the ratio of the magnetic Reynolds number to the viscous Reynolds number, R_m/R_e). Considering only the processes of Coulomb collisions in a fully ionized upper stellar convection zone, one can show $P_m \sim 1.3 \times 10^{-5} T^4/n$, where T is the temperature in K, and n is the number density of hydrogen atoms in cm^{-3} . Substituting typical values for T and n , one finds $P_m \ll 1$.

While a complete investigation of the dependence of our own convective dynamo on P_m is beyond the scope of this paper, as the simulation described above took 5–6 CPU months of computing resources, we have performed several exploratory calculations to get a rough idea of how the convective dynamo effectiveness depends on P_m . First, we have used the initial convective state of the dynamo run of this paper to explore how P_m affects the early growth phase of our convective dynamo. The result is that the growth rate decreases rapidly for $P_m \lesssim 2/3$, but shows signs of saturation for $P_m \gtrsim 2$. Second, we have used the saturated dynamo state of this paper as the initial condition for a series of simulations in which the same viscous Reynolds number is used, but where the magnetic Reynolds number has been changed, resulting in differing values of P_m . The convective dynamo then begins to relax to a new state that reflects the changed value of P_m . It appears that both the magnetic energy and the unsigned magnetic flux drop significantly for $P_m \lesssim 2/3$, but shows signs of saturation for $P_m \gtrsim 2$. Beyond this, for a fixed value of P_m , we also find evidence for a dependence on the magnetic or viscous Reynolds number due to the fact that we cannot simulate the full inertial range. We expect, as per the discussion below, that there will be an asymptotic limit to the kinetic and magnetic energies as the Reynolds numbers increase.

From this behavior, we conclude that for values of P_m much smaller than $2/3$ (for the range of magnetic and viscous Reynolds numbers that we can simulate), the convective dynamo is ineffective at generating magnetic energies that approach those of the kinetic energy of convection. We also conclude that values of $P_m \sim 1 - 2$ can generate significant amounts of magnetic energy and flux, with levels that are within a factor of ~ 10 of equipartition with kinetic energy. We speculate that larger values of P_m may to some degree increase the

effectiveness of the dynamo beyond the cases we can investigate here, but it seems unlikely that the dynamo can generate more magnetic energy than the kinetic energy equipartition value. Further, the simulations of Longcope, McLeish, & Fisher (2003), in which a closed magnetic ring is stretched by random convective motions, essentially has $P_m = \infty$ since the magnetic resistivity is zero in calculations like these. Yet these simulations still attain a finite amount of magnetic energy. In the large P_m limit, the field strength is most likely determined by a dynamic force balance between ram pressure gradients and magnetic tension forces, rather than by a balance between field amplification via stretching and field decay by magnetic diffusion, as occurs in the kinematic limit in many dynamo simulations.

Given the dependence of the convective dynamo on P_m that we seem to find, the small value of P_m set by collisional processes in stellar convection zones suggests that convective dynamos are extremely inefficient. However, a number of observational and theoretical considerations suggest the appropriate value for P_m is in fact much closer to unity in real stellar convection zones. We discuss these here.

First, magnetic elements on the Sun are observed to move, disperse, and cancel in response to granular and supergranular motions (Simon, Title, & Weiss 2001; Parnell 2002), indicating that long before the tiny molecular dissipation scales are reached, motions associated with convection can effectively disperse a magnetic element on much larger size scales. This means that the effective magnetic diffusivity is much larger than the molecular value. A similar argument applied to the observed correlation length and correlation time of convective motions also leads to a kinematic viscosity much greater than the molecular value, and qualitatively close to the effective magnetic diffusivity – implying a value of P_m near unity.

A related theoretical argument for $P_m \sim 1$ comes from two observations of our own simulations: (1) Both the magnetic and viscous Reynolds numbers of the real physical system we are attempting to model are far greater than those in our code. Therefore, at the smallest scale we can resolve in our code, magnetic fields and momentum are still well within the inertial range of the turbulent motions excited by convection, and therefore both momentum and magnetic fields will be diffused by eddies at the resolution scale and smaller. Applying a common eddy diffusivity for both quantities leads to a value of $P_m \sim 1$. A pitfall to this argument would occur if one could show that what occurred on sub-resolution scales could strongly affect what happens on the largest scales. This leads to our second observation: (2) Both the magnetic and kinetic energy spectra exhibit peaks at large scales, with significantly reduced energy at the smallest scales in the simulation, especially near the bottom of the simulation where the magnetic energy density is highest. Given this, it seems unlikely that details of the dissipation physics occurring on unresolved scales will have a strong effect on

the macroscopic properties of the dynamo simulation we have computed using $P_m = 4/3$. It is interesting to note that our conclusion that both magnetic and kinetic energies peak at large scales differs from the results of dynamo calculations using the “Kazantsev” approach, in which either the velocity (in kinematic models, e.g. Boldyrev & Cattaneo 2004) or an external force field (in dynamic models, e.g. Schekochihin et al. 2004) are driven by an assumed temporal white noise spectrum. Because our driving motions are computed self-consistently from the convection itself, and not from ad-hoc assumptions about a forcing term, we feel we have applied our results in a physically self-consistent manner by assuming a value of P_m near unity.

There are other theoretical arguments against using the molecular diffusivities. Longcope, McLeish, & Fisher (2003) argue that the presence of fibril magnetic fields in the convection zone plasma results in an effective viscosity that is at least as great as the turbulent viscosity, if not larger. Abbett et al. (2004) show that magnetic flux tubes are dispersed in a model convection zone with an effective magnetic diffusivity given by a turbulent eddy diffusivity.

Taken together, all of these results argue for a common eddy diffusivity for both processes and therefore a magnetic Prandtl number near unity. We adopt $P_m = 4/3$ instead of unity simply because we want to choose the largest possible values of the viscous and magnetic Reynolds numbers that do not result in numerical artifacts. Our preliminary calculations indicate no significant differences between using results from $P_m = 4/3$ versus assuming a value of unity.

3. Connecting the Dynamo Model to the Stellar Envelope

Here, we relate the anelastic simulation results described in §2, which are performed in dimensionless units, to physical units so that the resulting magnetic surface flux can be compared with stellar observations. We must therefore assign cgs units to the non-dimensional simulation results and connect the velocity and magnetic fields of the simulation to the luminosity, surface gravity, radius, effective temperature and surface density of main sequence reference stars.

The variation of the background temperature $T_0(z)$ and density $\rho_0(z)$ with height z above the base of our anelastic simulation box is taken to be a polytrope with index $m = 1/(\gamma - 1) = 1.5$ (here γ refers to the adiabatic index for an ideal gas) and is given explicitly by

$$T_0(z) = T_{\text{ref}} \left[1 - \frac{z}{(m+1)H_{\text{ref}}} \right] \quad (2)$$

and

$$\rho_0(z) = \rho_{\text{ref}} \left(\frac{T_0(z)}{T_{\text{ref}}} \right)^m. \quad (3)$$

Here, the subscript “ref” denotes chosen reference values at the base of the box (see Fan, Abbett, & Fisher 2003). Values of the thermodynamic variables at the top (or surface) of the box are denoted with a subscript “surf”. The ratio $T_{\text{ref}}/T_{\text{surf}}$ is one of the fixed parameters in the simulation described in this paper, and is set to 7.8, and results in a stratified background atmosphere with a base-to-surface density ratio $\rho_{\text{ref}}/\rho_{\text{surf}}$ of 21.8 and a corresponding pressure ratio $P_{\text{ref}}/P_{\text{surf}}$ of 170.6. The reference temperature T_{ref} at the base is determined from the effective surface temperature T_{eff} by setting $T_{\text{surf}} = T_{\text{eff}}$, and then using the fixed ratio $T_{\text{ref}}/T_{\text{surf}}$ to determine the actual value of T_{ref} in degrees K. Similarly, the value of surface density from stellar atmosphere models, along with equation 3 is used to determine the reference density ρ_{ref} .

In the anelastic simulation, the unit of length is the pressure scale height at the base of the domain, $H_{\text{ref}} \equiv RT_{\text{ref}}/(\bar{\mu}g_{\text{ref}})$, where R is the universal gas constant, $\bar{\mu}$ is the mean molecular weight, and g_{ref} is the value of the gravitational acceleration at the base of the simulation box. For simplicity, we assume that $\bar{\mu} = 0.5$, which corresponds to a fully ionized hydrogen gas. Near the surface of the later type stars we consider, the gas will be nearly neutral, however. Our neglect of the effects of variable ionization in the background atmosphere is a limitation of our current calculations that could be improved in future work. We assume that the values of g_{ref} and g_{surf} , the surface gravitational acceleration, are equal, since the depth of the box is quite small compared to a stellar radius for the cases we consider. The depth of the box \mathcal{L}_z is given by

$$\mathcal{L}_z = (m + 1) \frac{T_{\text{ref}} - T_{\text{surf}}}{T_{\text{ref}}} H_{\text{ref}}, \quad (4)$$

and the horizontal dimensions of the box, \mathcal{L}_x and \mathcal{L}_y are four times larger than \mathcal{L}_z .

The unit of velocity in the simulations is defined in terms of a dimensionless entropy gradient (see § 2). To convert the velocity units to physical values, we note that in our simulation, the dominant form of energy transport from the base to the top is thermal convection. We therefore require that the vertical energy flux match that needed to carry the stellar luminosity in a particular stellar model. In other words, for a given star with luminosity L_\star and radius R_\star , the energy flux carried by convection in the outer convective envelope must be given by

$$F_{\text{conv}} = \frac{L_\star}{4\pi R_\star^2}. \quad (5)$$

We have assumed that throughout the convective envelope, the fraction of energy carried by radiative diffusion is far less than that carried by convection, which is a reasonable assumption.

tion for the stars we consider here. This assumption will break down near the photosphere, where radiation begins to dominate.

To estimate F_{conv} in a consistent way that applies to each of the different stellar types we consider, we use a simple form of mixing length theory to obtain an approximate reference value of the convective velocity at the depth corresponding to the base of our simulation domain. Here, we adopt the mixing length formulation of Mihalas (1978). Combining his equations 7-68 and 7-69, and explicitly evaluating C_p as $5R/(2\bar{\mu})$, we find

$$F_{\text{conv}} = \frac{10}{\alpha} \rho v_{\text{conv}}^3, \quad (6)$$

where ρ is the background density of the convective envelope, v_{conv} is the characteristic convective velocity, and $\alpha = l/H_p$ is the ratio of the “mixing length” to the pressure scale height. While mixing length theory is a crude approximation, it has been shown to provide roughly the right velocity amplitude in simulations of realistic surface convection (Abbett et al. 1997), who also find best results when $\alpha \sim 1.5$. Our use of equation 6 is to take the stellar value of F_{conv} and the background stratification of ρ to estimate the value of v_{conv} at the base of our simulation (which we will take as the reference value v_{ref}), and to then assume that our simulation velocity is measured in units of this value. If desired, one can work backwards to determine the corresponding entropy gradient, but this is not necessary. We have used equations 5 and 6 to estimate the convective velocity in the layers just below the solar photosphere and find values of $\sim 3 \text{ km s}^{-1}$, in approximate agreement with much more detailed models of the solar interior (see e.g., Abbett et al. 1997; Stein & Nordlund 1998; Asplund et al. 2000; Samadi et al. 2003), and with observations of convective velocities from granulation (Hirzberger et al. 2001; Roudier et al. 2003).

Because the depth of our simulation box is small compared to the stellar radius in all the cases we consider, we are justified in ignoring the change in radius with depth and assume that F_{conv} is uniform with depth within the box. This means that v_{conv} at the base of the box (i.e., v_{ref}) can be found from equations 2, 3, 5, and 6, and is given by

$$v_{\text{ref}} = v_{\text{surf}} \left(\frac{T_{\text{surf}}}{T_{\text{ref}}} \right)^{\frac{m}{3}}, \quad (7)$$

where

$$v_{\text{surf}} = \left(\frac{\alpha L_{\star}}{40\pi \rho_{\text{surf}} R_{\star}^2} \right)^{\frac{1}{3}}. \quad (8)$$

Note that equation 7 is extremely insensitive to the precise formulation used in the mixing length theory. For example, if the coefficient “10” in equation 6 was changed by a factor of ten, it would result in only a factor of 2.15 difference in the resulting value of v_{ref} .

The magnetic field strengths of the simulation are given in units of

$$B_{\text{ref}} = (4\pi\rho_{\text{ref}})^{\frac{1}{2}}v_{\text{ref}}. \quad (9)$$

To convert to physical units (G), we simply substitute the expression for v_{ref} (equation 7) into equation 9:

$$B_{\text{ref}} = \left[\frac{\pi^{\frac{1}{2}}\alpha L_{\star}}{5R_{\star}^2} \right]^{\frac{1}{3}} \rho_{\text{surf}}^{\frac{1}{6}} \left[\frac{T_{\text{ref}}}{T_{\text{surf}}} \right]^{\frac{m}{6}}. \quad (10)$$

The scaling relationships given here allow us to estimate the amount of magnetic flux and the mean field strength near the top of our anelastic simulation of the turbulent dynamo. We note that although the anelastic formulation is not well suited to modeling the surface layers of stellar atmospheres, and that the convection in our simulations is not driven explicitly by radiative cooling in the surface layers, our simulation remains appropriate for our study since we are only interested in obtaining an estimate of the total magnetic flux threading the top of the convective envelope — not the detailed dynamics or distribution of magnetic fields across a stellar photosphere. Table 1 lists the parameters used to calculate the scaling of the simulation results for a sample of main sequence stars ranging in spectral type from F0 to M0. All stellar parameters except surface density are taken from Gray (1992) for spectral types F0–K5, and those for M0 are taken from Reid & Hawley (2000). The surface densities (column 6 of Table 1) are evaluated at the depth where the local temperature is equal to the effective temperature (column 2) using model atmospheres from Kurucz (1993).

4. Results

We have generated significant magnetic fields (via a convective dynamo) in a stratified turbulent model convection zone by imposing a dynamically insignificant seed field on a statistically relaxed convective state. Our treatment differs from that of Cattaneo (1999), since our domain is highly stratified; however, the energetics of our simulation are similar to his results — we find that the magnetic field fully saturates at roughly seven percent of the total kinetic energy of the computational domain. We find that the magnetic filling factor is small near the surface, and larger deeper in the convective envelope, and that the total amount of unsigned magnetic flux is concentrated in the lower half of the simulation domain. Strong fields are concentrated and highly localized, while weaker fields are more evenly distributed. We also note that the correlation time of magnetic flux structures near the top of the simulation box is $2\text{--}3 H_{\text{ref}}/v_{\text{conv}}$, which corresponds to 1–2 hours for a solar-type star.

The results of applying the $\alpha = 1.5$ mixing length scaling to the simulation data are presented in columns 2–4 of Table 2: column 2 lists the pressure scale height at the base of the domain, column 3 lists the convective velocities at the surface, and column 4 lists the total magnetic fluxes of the reference stars, Φ_* . The magnetic fluxes were obtained by first averaging the total unsigned flux through a horizontal layer near the top of the simulation box ($z = z_u$) over an interval $250 H_{\text{ref}}/v_{\text{conv}}$ centered at $t = 725 H_{\text{ref}}/v_{\text{conv}}$ (see Figure 1). The simulated result was then scaled from the horizontal area of the computational domain to the surface area of the reference stars. Here, we assume that all areas on the stellar surface are uncorrelated and generate magnetic field in the same way and with the same efficiency.

We estimate the X-ray luminosities of the reference stars through an empirical relationship between the X-ray luminosity and unsigned magnetic flux (Pevtsov et al. 2003). A fit to the data presented in Figure 1 of that paper leads to the relation

$$L_X = 0.8940 \Phi_*^{1.1488}. \quad (11)$$

The X-ray luminosity, L_X , and surface X-ray flux, F_X , for our sample of reference stars are listed columns 4 and 5 of Table 2, respectively.

We compare the results of our simulation to the volume limited sample of cool stars discussed in Schmitt (1997). The stellar data itself comes from both Schmitt, Fleming, & Giampapa (1995) and Schmitt (1997). These papers provide the X-ray luminosity and either the absolute visual magnitude, M_V , or the spectral type and M_V for each star. The observed $B - V$ is also given for about half the stars in the sample. The spectral type (if given) or M_V is converted to a $B - V$ index (if needed) and a stellar radius using the main sequence calibration given by Gray (1992) for stars K7 and earlier, or that given by Reid & Hawley (2000) for stars M0 and later. In the case of the M dwarfs, Reid & Hawley (2000) do not give a direct spectral type — M_V (or $B - V$) calibration, so we used the data provided in their appendices to construct one. We binned the stellar data for the 8 pc sample into spectral type bins (M0, M0.5, M1, M1.5, ...) and averaged the values of M_V and $B - V$ in each bin. These averages were then fit with a 5th-order polynomial to construct our final M dwarf calibration of M_V and $B - V$ as a function of spectral type. Using the published X-ray luminosities and our calculated stellar radii, we then found the X-ray surface flux for each observed star (shown as a filled circle in Figure 6). Our predicted model surface fluxes calculated using a mixing length parameter $\alpha = 1.5$ are shown with asterisks connected by a dashed line in the same figure. The gray region shows the range of the predicted surface X-ray fluxes if the convective flux calculated by the models varies by a factor of eight (or equivalently if the velocity scaling varies by a factor of two) above or below that calculated using $\alpha = 1.5$.

It is reasonable to assume that the heating mechanism that produces X-ray emission

also produces emission in chromospheric and transition region diagnostics, contributing to the basal emission level observed in these lines. Without a detailed magnetic heating model, we can only explore this issue using flux-flux relationships between X-ray emission and diagnostics such as Mg II emission. Many investigators have found good correlation between these diagnostics, and here we use the flux-flux relationship

$$\log F_{\text{Mg II}} = \frac{\log F_X}{1.97} + \frac{6.7}{1.97} \quad (12)$$

based on Table 4 of Rutten et al. (1991) to determine an estimate of Mg II emission for our reference stars.

Rutten et al. (1991) do not find a basal emission level in their X-ray observations, but do find one in the Mg II emission which they attribute to acoustic heating. Subtracting off this basal emission from observed Mg II emission for all stars then improves the correlation of Mg II with X-ray emission. The assumption is that this excess Mg II emission is all magnetic in origin, as is the X-ray emission. Since the emission we calculate is explicitly magnetic in origin, we use the relationship between excess Mg II emission and X-ray emission (column b of Table 4 in Rutten et al. 1991). We note though, that using the total flux-flux relationship given in Rutten et al. (1991) increases the predicted Mg II emission by only ~ 0.2 dex, which is well within the range of variation shown in the plots for different choices of the mixing length in our magnetoconvection simulations. Since our predicted X-ray surface fluxes do not depend strongly on stellar $B-V$, it is not surprising that we find a similarly weak dependence on stellar spectral type of the resulting Mg II surface flux: we find $\log(F_{\text{Mg II}}) = 5.50$ at F0 and 5.34 at M0.

At first glance, these values appear inconsistent with the basal flux observations of Rutten et al. (1991) (their figure 1b), where the basal level appears to be $\log(F_{\text{Mg II}}) \sim 4.5$ at $B - V = 1.5$. However, a closer inspection of this figure (indeed, of all the flux-color figures in Rutten et al. (1991)) shows that the lower limit to the Mg II emission is defined by giants and subgiants at later spectral types. The dwarf stars are all significantly stronger than the apparent lower limit at these later spectral types. In addition, there is no apparent piling up of the dwarf star observations against a lower bound as would be expected for basal emission (see Schrijver 1995), probably due in part to the small number of dwarf stars observed by Rutten et al. (1991) (there are only 13 stars later than $B - V = 1.0$ in their Figure 1b). This lack of piling up of the dwarfs is apparent across all $B - V$ (0.3 to 1.5) plotted in Rutten et al. (1991). A more complete survey of Mg II emission in K and M dwarf stars is provided by Mathioudakis & Doyle (1992). In Figure 7 we plot the Mg II surface flux on the dK and dM stars from Tables 1 and 2 of Mathioudakis & Doyle (1992) against their observed $B - V$ (we do not plot the dKe and dMe stars as these stars are expected to — and do — show much stronger emission than that from basal emission stars). Also shown

in Figure 7 is our predicted Mg II surface flux based on our dwarf models from equation 12. Our predicted emission levels due to a convective dynamo fall nicely at the lower limit of the observed emission in the range that the models are valid ($B - V < 1.5$). The agreement seen in Figure 7 is substantially better than that shown in the acoustic heating models of Buchholz, Ulmschneider, & Cuntz (1998), whose predicted surface fluxes are too weak ($\log(F_{\text{Mg II}}) = 4.6$ to 4.8 at $B - V = 1.4$) and show a much stronger color dependence (for $B - V < 1.4$) than seen in the dwarf star observations of Mathioudakis & Doyle (1992) or seen in the dwarf star observations of Rutten et al. (1991). On the other hand, at earlier spectra types ($B - V \lesssim 0.5$) the acoustic heating models better match the lower bound of the Mg II observations than the crude estimates presented here.

As discussed in § 2, the overall flux achieved in our convective dynamo simulations does depend on the value of the magnetic Prandtl number P_m . However, the scaling of the model to main sequence stars of different spectral types does not—the resulting weak color dependence of the X-ray and Mg II emission is independent of P_m , whereas acoustic heating models show a strong color dependence. The X-ray data (Figure 6) and the more complete Mg II data (Figure 7) show a weak color dependence over the spectral type range in our models that is consistent with the convective dynamo predictions and not with the acoustic model predictions.

5. Discussion and Conclusions

We have performed 3D MHD simulations of a turbulent dynamo in a highly stratified Cartesian domain in order to determine the amount and distribution of magnetic flux generated in a non-rotating convective envelope. We use the computed surface flux near the upper boundary of the domain and an empirical relationship between magnetic flux and X-ray flux (Pevtsov et al. 2003) to determine the lower limit of X-ray emission in main sequence stars. Figure 6 suggests that our simple analytic scaling treatment successfully reproduces the observed lower limit of X-ray flux found by Schmitt (1997) in the range from F0–M0. This result suggests that the level of heating by magnetic sources in the coronae of these stars is sufficient to account for most if not all of the X-ray flux.

Stars earlier than spectral type F0 are expected to have the thicknesses of their outer convective shells rapidly decrease to zero as the surface temperature increases. The low surface X-ray fluxes for the three observed stars for which $B - V < 0.1$ are consistent with less heating due to a diminished level of magnetic field generated by the convective dynamo; however, the same argument holds for less heating due to a diminished convective acoustic flux. We do not extend our treatment to spectral types later than M0, since we expect that

our assumptions of an ideal equation of state and high electrical conductivity will break down for cool M dwarf atmospheres. Our treatment implicitly assumes that the Pevtsov et al. (2003) relation applies to magnetic flux generated by the turbulent convective dynamo. Currently, the best hope for verifying this assumption is forward modeling of coronal heating of ensembles of magnetic loops (e.g., Lundquist et al. 2004; Schrijver et al. 2004), as well as in understanding the role of sub-pixel magnetic structures on measured magnetic flux densities.

We use the flux-flux relation of Rutten et al. (1991) to determine the expected level of chromospheric emission in Mg II. For K dwarfs we find good agreement with the observed lower limit of Mg II surface flux in the K dwarf sample of Mathioudakis & Doyle (1992), suggesting that this observed lower limit is entirely the result of magnetic heating. On the other hand, our models predict a very shallow dependence of both X-ray and Mg II emission with spectral type, so that they underestimate the Mg II emission at earlier spectral types (though our models are a good match to the X-ray emission at these spectral types). This suggests some other agent (acoustic heating) is required to produce the minimum observed Mg II emission at earlier spectral types, and that this additional mechanism produces relatively little X-ray emission. At the very latest spectral types, the sharp drop in the Mg II surface flux seen in Figure 7 at $B - V \sim 1.5$ suggests something very different may be happening here. We do not expect our models to be valid at these cool temperatures due to the relatively low ionization that will result. In addition, the X-ray emission from stars observed in Figure 6 does not show this same drop, indicating that the flux-flux calibration used to predict the Mg II emission based on the X-ray emission will not hold. We cannot address the level of acoustic heating with our dynamo model. Obviously, if there is convection there will be some level of acoustic activity. However, the results we present here provide a consistent and viable alternative to acoustic heating for K type dwarfs in the absence of a large scale dynamo. At earlier spectral types, our results suggest turbulent dynamos can also fully account for the lower limit to the observed X-ray emission, though there may still be a substantial acoustic contribution to the coronal emission in earlier type stars.

This work was supported by NASA’s Astrophysics Theory Program through the grant “Three Dimensional MHD Simulations of Turbulent Dynamos in Convecting Stars”. In addition, W. P. A. and G. H. F. were supported by NASA through the SEC SR&T grant “The Physics of Active Regions”, and through the DoD MURI grant, “Understanding Magnetic Eruptions on the Sun and their Interplanetary Consequences”. C. M. J.-K. would like to acknowledge partial support from the NASA Origins program through grant number NAG5-13103. We wish to thank Gibor Basri, Yuhong Fan, Alex Pevtsov, Karel Schrijver, Bob Stein and the referee for helpful comments and discussions.

REFERENCES

- Abbett, W. P., Beaver, M., Davids, B., Georgobiani, D., Rathbun, P., & Stein, R. F. 1997, *ApJ*, 480, 395
- Abbett, W. P., Fisher, G. H., Fan, Y., & Bercik D. J. 2004, *ApJ*, 612, 557
- Asplund, M., Ludwig, H.-G., Nordlund, Å., & Stein, R. F. 2000, *A&A*, 359, 669
- Basri, G. 1987, *ApJ*, 316, 377
- Boldyrev, S., & Cattaneo, F. 2004, *Phys. Rev. Lett.*, 92, 144501
- Buchholz, B., Ulmschneider, P., & Cuntz, M. 1998, *ApJ*, 494, 700
- Bueno, J. T., Shchukina, N., & Ramos, A. A. 2004, *Nature*, 403, 326
- Cattaneo, F. 1999, *ApJ*, 515, L39
- Dorch, S. B. F. 2004, *A&A*, 423, 1101
- Durney, B. R. & Latour, J. 1978, *Geophys. Astrophys. Fluid Dyn.*, 9, 241
- Durney, B. R., De Young, D. S., & Roxburgh, I. W. 1993, *Sol. Phys.*, 145, 207
- Emonet, T. & Cattaneo, F. 2001, *ApJ*, 560, L197
- Fan, Y. 2004, *Living Rev. Solar Phys.*, 1, 1
- Fan, Y., Zweibel, E. G., Linton, M. G., & Fisher, G. H. 1999, *ApJ*, 521, 460
- Fan, Y., Abbett, W. P., & Fisher, G. H. 2003, *ApJ*, 582, 1206
- Fisher, G. H., Longcope, D. W., Metcalf, T. R., & Pevtsov, A. A. 1998, *ApJ*, 508, 885
- Fisher, G. H., Fan, Y., Longcope, D. W., Linton, M. G., & Pevtsov, A. A. 2000, *Sol. Phys.*, 192, 119
- Giampapa, M. S., Rosner, R., Kashyap, V., Fleming, T. A., Schmitt, J. H. M. M., & Bookbinder, J. A. 1996, *ApJ*, 463, 707
- Gough, D. O. 1969, *J. Atmos. Sci.*, 26, 448
- Gray, D. F. 1992, *The Observation and Analysis of Stellar Photospheres* (2nd ed.; Cambridge: Cambridge Univ. Press)

- Hagenaar, H. J., Schrijver, C. J., & Title, A. M. 2003, *ApJ*, 584, 1107
- Harvey, K. L. 1993, Ph.D. Thesis, Univ. Utrecht
- Hirzberger, J., Koschinsky, M., Kneer, F., & Ritter, C. 2001, *A&A*, 367, 1011
- Johns-Krull, C. M. 1996, *A&A*, 306, 803
- Johns-Krull, C. M., Valenti, J. A., & Linsky, J. L. 2000, *ApJ*, 539, 815
- Judge, P. G. & Carpenter, K. G. 1998, *ApJ*, 494, 828
- Khomenko, E. V., Collados, M., Solanki, S. K., Lagg, A., & Trujillo Bueno, J. 2003, *A&A*, 408, 1115
- Küker, M. & Rüdiger, G. 1999, *A&A*, 346, 922
- Kurucz, R. L. 1993, ATLAS9 Stellar Atmosphere Programs and 2 km/s grid, Kurucz CD-ROM No. 13 (Cambridge, Mass.: SAO)
- Lantz, S. R., & Fan, Y. 1999, *ApJS*, 121, 247
- Lin, H. & Rimmele, T. 1999, *ApJ*, 514, 448
- Longcope, D. W., McLeish, T. C. B., & Fisher, G. H. 2003, *ApJ*, 599, 661
- Lundquist, L. L., Fisher, G. H., McTiernan, J. M., & Régnier, S. 2004, “Using Synthetic Emission Images to Constrain Heating Parameters”, in “Proceedings of the SOHO 15 Workshop”, in press.
- Mathioudakis, M. & Doyle, J. G. 1992, *A&A*, 262, 523
- Meneguzzi, M. & Pouquet, A. 1986, in *Reconnection and Turbulence*, ed. M. A. Dubois, D. Grélon, & M. N. Bussac (Orsay: Les Editions de Physique), 109
- Mewe, R., Schrijver, C. J., & Zwaan, C. 1981, *Space Sci. Rev.*, 30, 191
- Mihalas, D. 1978, *Stellar Atmospheres* (2nd ed.; San Francisco: W. H. Freeman and Company)
- Mullan, D. J. & Cheng, Q. Q. 1994, *ApJ*, 420, 392
- Mullan, D. J. & Cheng, Q. Q. 1994, *ApJ*, 435, 435
- Mullan, D. J. & Fleming, T. A. 1996, *ApJ*, 464, 890

- Noyes, R. W., Hartmann, L. W., Baliunas, S. L., Duncan, D. K., & Vaughan, A. H. 1984, *ApJ*, 279, 763
- Parnell, C. E. 2002, *MNRAS*, 335, 389
- Pevtsov, A. A., Fisher, G. H., Acton, L. W., Longcope, D. W., Johns-Krull, C. M., Kankelborg, C. C., & Metcalf, T. R. 2003, *ApJ*, 598, 1387
- Pevtsov, A. A. 2004, private communication.
- Reid, N. I. & Hawley, S. L. 2000, *New Light on Dark Stars* (New York: Springer)
- Roudier, T., Malherbe, J. M., Mein, P., Muller, R., Coutard, C., Lafon, M., & Grimaud, F. 2003, *A&A*, 409, 793
- Rüdiger, G. 1989, *Differential Rotation and Stellar Convection* (Berlin: Akademie-Verlag), chap. 4
- Rutten, R. G. M. 1984, *A&A*, 130, 353
- Rutten, R. G. M., Schrijver, C. J., Lemmens, A. F. P., & Zwaan, C. 1991, *A&A*, 252, 203
- Samadi, R., Nordlund, Å., Stein, R. F., Goupil, M. J., & Roxburgh, I. 2003, *A&A*, 403, 303
- Schekochihin, A. A., Haugen, N. E. L., Brandenburg, A., Cowley, S. C., Maron, J. L., & McWilliams, J. C. 2004, preprint (astro-ph/0412594)
- Schmitt, J. H. M. M., Fleming, T. A., & Giampapa, M. S. 1995, *ApJ*, 450, 392
- Schmitt, J. H. M. M. 1997, *A&A*, 318, 215
- Schrijver, C. J. 1983, *A&A*, 127, 289
- Schrijver, C. J. 1987, *A&A*, 172, 111
- Schrijver, C. J. 1995, *A&A Rev.*, 6, 181
- Schrijver, C. J., Dobson, A. K., & Radick, R. R. 1989, *ApJ*, 341, 1035
- Schrijver, C. J., Sandman, A. W., DeRosa, M. L., & Aschwanden, M. J. 2004, *American Astronomical Society Meeting*, 204
- Simon, G. W., Title, A. M., & Weiss, N. O. 2001, *ApJ*, 561, 427
- Skumanich, A. 1972, *ApJ*, 171, 565

- Stein, R. F. & Nordlund, A. 1998, *ApJ*, 499, 914
- Tanner, S. E. M. & Hughes, D. W. 2003, *ApJ*, 586, 685
- Thelen, J.-C. & Cattaneo, F. 2000, *MNRAS*, 315, L13
- Title, A. M. & Schrijver, C. J. 1998, in *ASP Conf. Ser. 154: Tenth Cambridge Workshop on Cool Stars, Stellar Systems and the Sun*, ed. R. A. Donahue & J. A. Bookbinder (San Francisco: ASP), 345
- Tobias, S. M., Brummell, N. H., Clune, T. L., & Toomre, J. 2001, *ApJ*, 549, 1183
- Vainshtein, S. I., Sagdeev, R. Z., Rosner, R., & Kim, E. 1996, *Phys. Rev. E*, 53, 4729
- Vaughan, A. H., Preston, G. W., & Wilson, O. C. 1978, *PASP*, 90, 267
- Vilhu, O. 1984, *A&A*, 133, 117

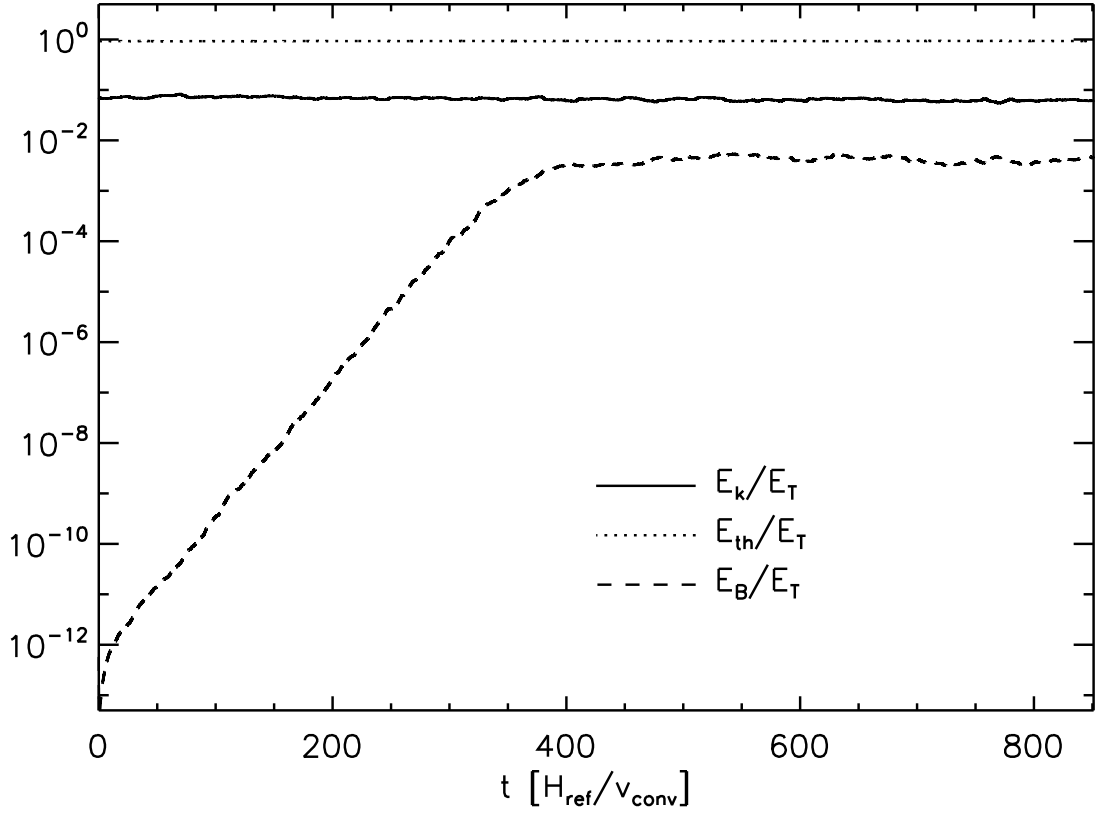


Fig. 1.— Shown are the kinetic (solid line), thermal (dotted line), and magnetic (dashed line) energy fluctuations (normalized by the sum of the three) as a function of time (in units of $H_{\text{ref}}/v_{\text{conv}}$).

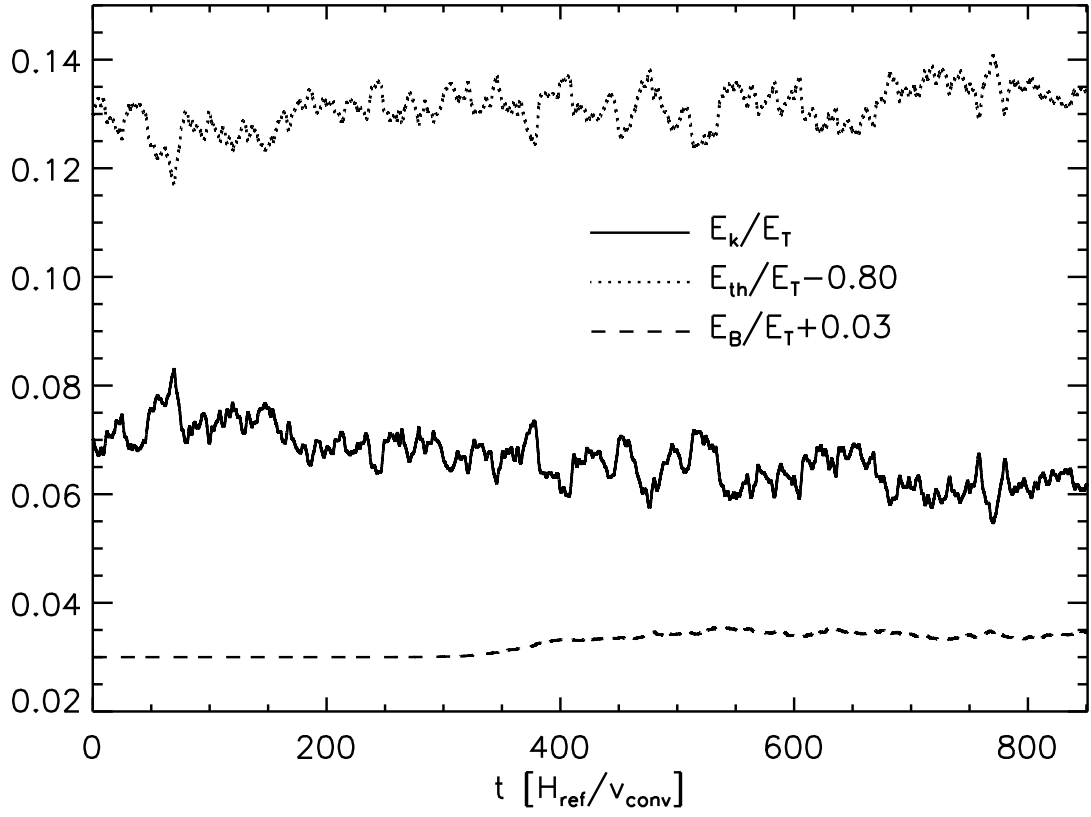


Fig. 2.— Same as Figure 1 except on a linear scale. To facilitate comparison, the magnetic and thermal energies are vertically shifted.

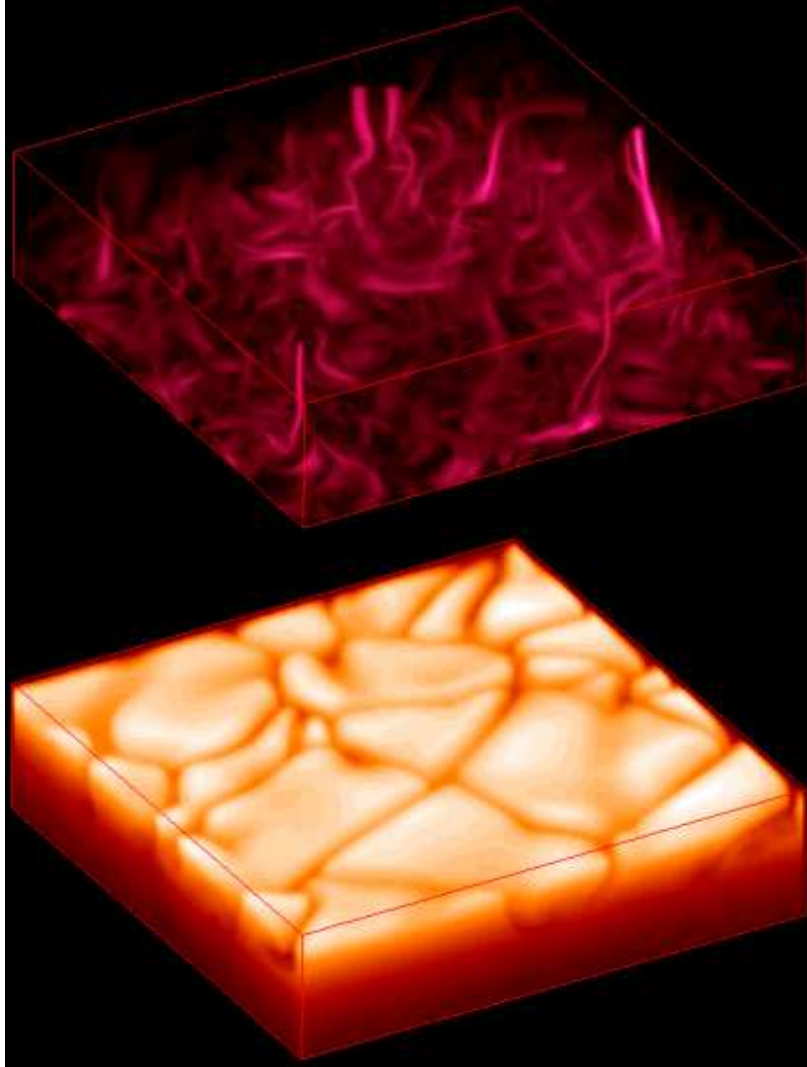


Fig. 3.— Volume rendering of the magnetic field strength $|\mathbf{B}|$ (upper frame) and the corresponding entropy perturbations (lower frame) at $t = 710 H_{\text{ref}}/v_{\text{conv}}$ (well after saturation).

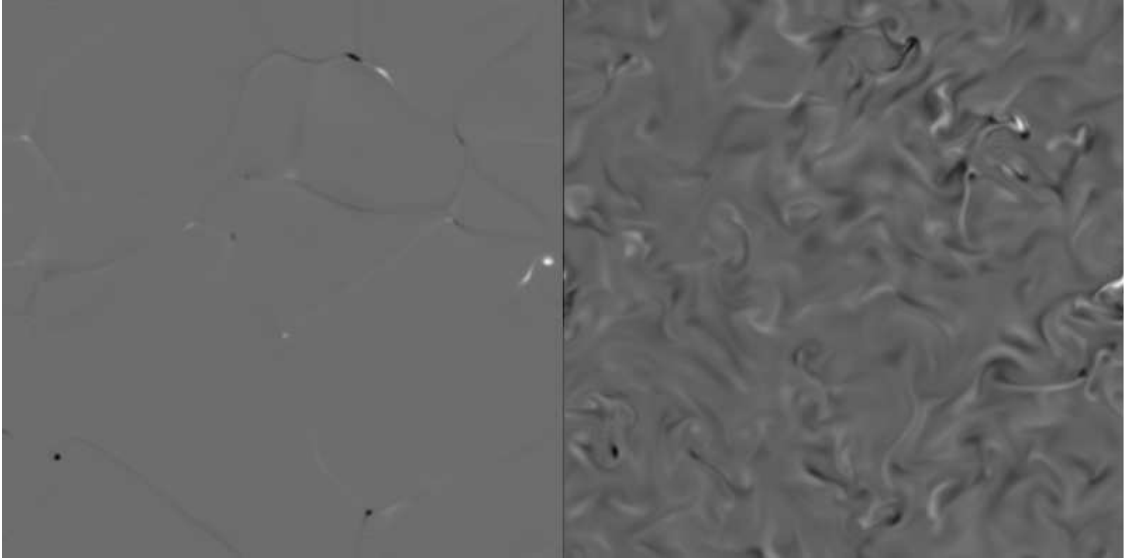


Fig. 4.— The vertical component of the magnetic field at $t = 710 H_{\text{ref}}/v_{\text{conv}}$ along a horizontal slice taken at $z_u = 2.06 H_{\text{ref}}$ near the top of the simulation domain (left frame), and at and $z_l = 0.45 H_{\text{ref}}$ near the bottom (right frame).

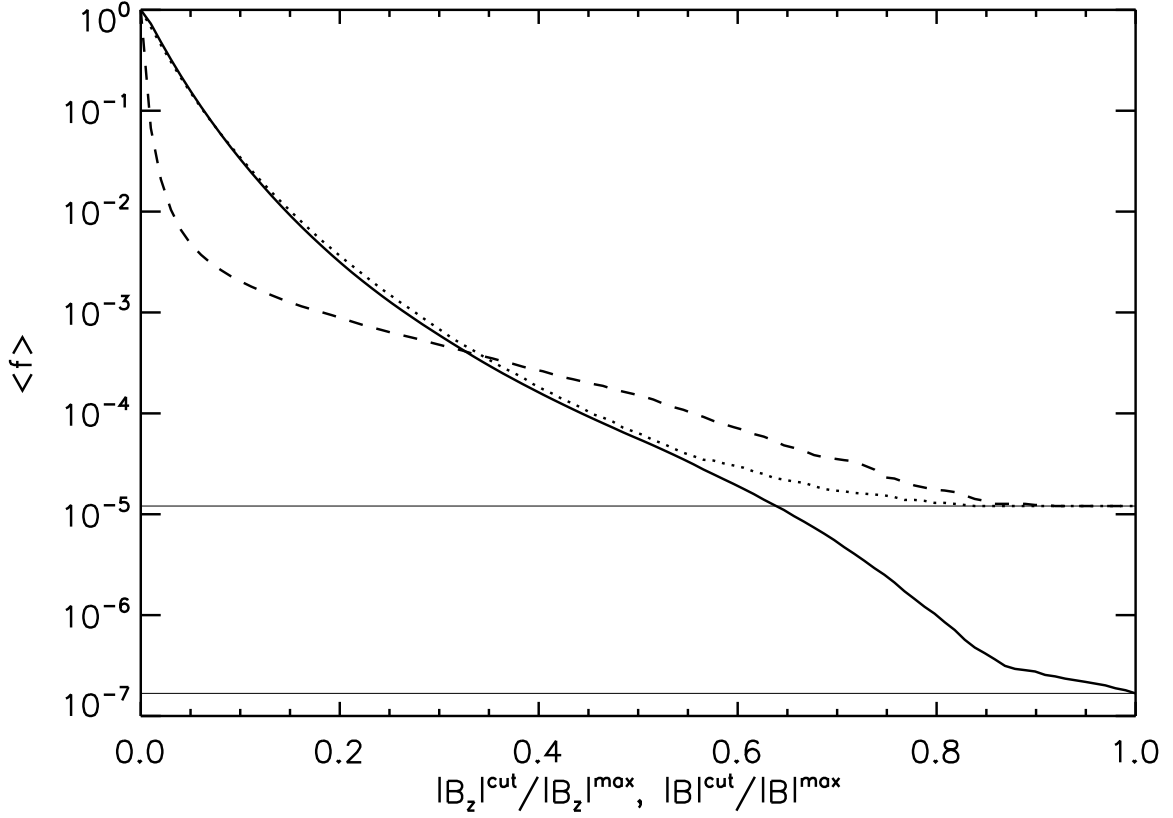


Fig. 5.— The time-averaged filling factor $\langle f \rangle$ as a function of $|B_z|^{\text{cut}}/|B_z|^{\text{max}}$ for two horizontal slices through the domain: near the top (dashed line), and near the bottom (dotted line). Also shown is the volumetric filling factor over the entire domain (solid line). The thin straight lines represent the one count per area and one count per volume baselines. See text for details.

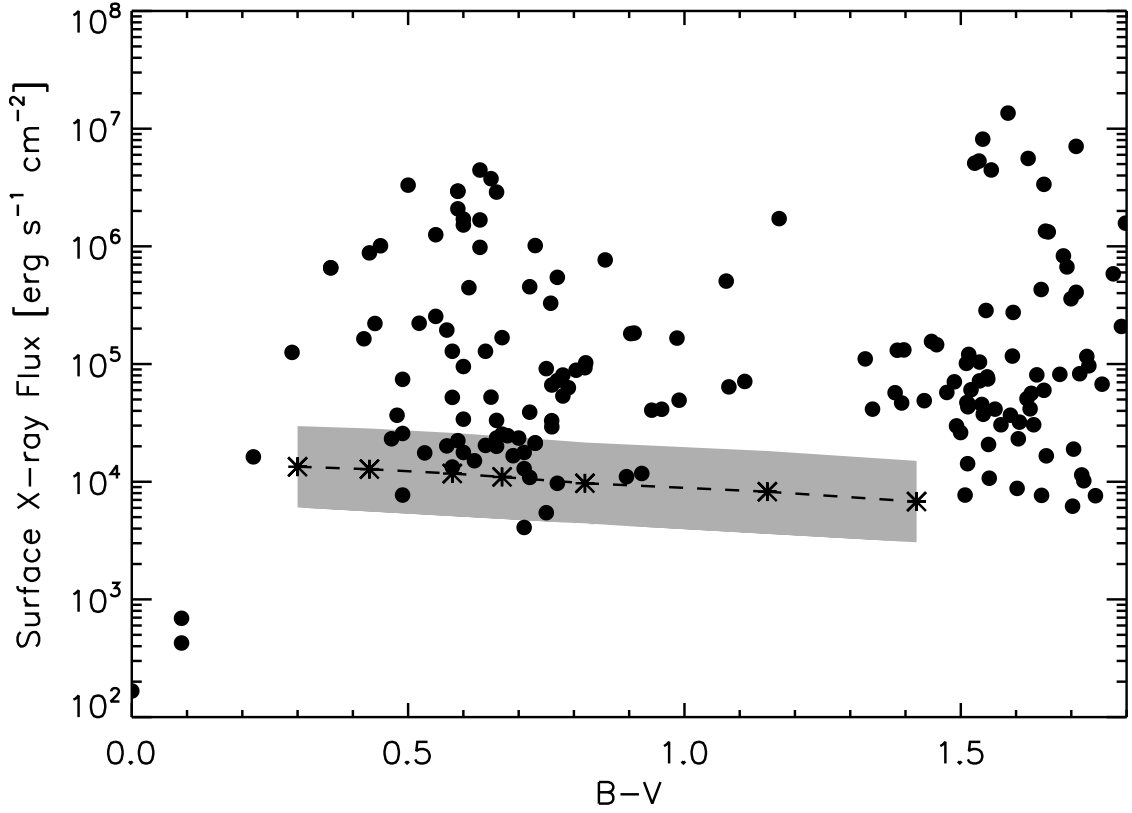


Fig. 6.— The filled circles represent the X-ray surface flux for each observed star as a function of $B - V$ color. The asterisks represent our theoretical prediction of the lower bound of the X-ray surface flux for a choice of mixing length parameter $\alpha = 1.5$. The gray shaded area indicates the amount that these levels can change if the assumed surface velocities change by a factor of two. See text for details.

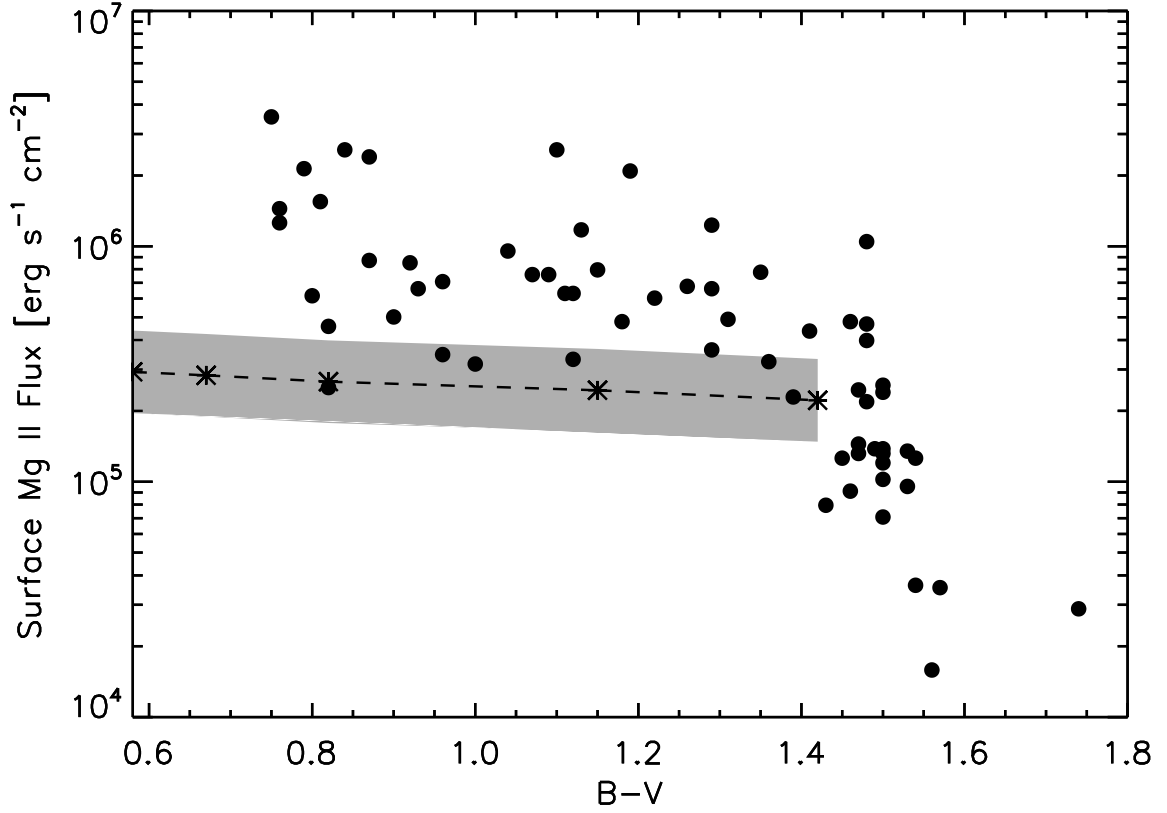


Fig. 7.— The filled circles represent the Mg II surface flux for each observed star as a function of $B - V$ color. The asterisks represent our theoretical prediction of the lower bound of the Mg II surface flux for a choice of mixing length parameter $\alpha = 1.5$. The gray shaded area indicates the amount that these levels can change if the assumed surface velocities change by a factor of two. See text for details.

Table 1. Stellar model parameters

Spectral Type	T_{eff} [K]	L_{\star} [erg s $^{-1}$]	R_{\star} [cm]	$\log g$ [cm s $^{-2}$]	ρ_{surf} [g cm $^{-3}$]
F0	6949	1.84×10^{34}	1.05×10^{11}	4.27	6.71×10^{-8}
F5	6445	1.04×10^{34}	9.19×10^{10}	4.32	1.18×10^{-7}
G0	5948	5.04×10^{33}	7.52×10^{10}	4.42	1.97×10^{-7}
G5	5678	3.31×10^{33}	6.68×10^{10}	4.46	2.42×10^{-7}
K0	5273	1.75×10^{33}	5.64×10^{10}	4.53	3.02×10^{-7}
K5	4557	6.88×10^{32}	4.73×10^{10}	4.60	5.33×10^{-7}
M0	3800	2.77×10^{32}	4.32×10^{10}	4.65	9.60×10^{-7}

Table 2. Scaled results for $\alpha = 1.5$

Spectral Type	H_{ref} [Mm]	v_{surf} [km s $^{-1}$]	Φ_{\star} [Mx]	L_{X} [erg s $^{-1}$]	$\log F_{\text{X}}$ [erg s $^{-1}$ cm $^{-2}$]
F0	4.86	6.67	6.01×10^{23}	1.86×10^{27}	4.13
F5	4.02	4.99	4.57×10^{23}	1.36×10^{27}	4.11
G0	2.95	3.78	2.99×10^{23}	8.34×10^{26}	4.07
G5	2.56	3.32	2.30×10^{23}	6.16×10^{26}	4.04
K0	2.03	2.79	1.54×10^{23}	3.88×10^{26}	3.99
K5	1.49	1.90	9.81×10^{22}	2.31×10^{26}	3.92
M0	1.11	1.23	7.08×10^{22}	1.59×10^{26}	3.83